Smart Structures and Systems, *Vol. 26, No. 5 (2020) 545-558*
DOI: https://doi.org/10.12989/sss.2020.26.5.545

Optimal design of multiple tuned mass dampers for vibration control of a cable-supported roof

X.C. Wang, Q. Teng*, Y.F. Duan**, C.B. Yun, S.L. Dong and W.J. Lou

College of Civil Engineering and Architecture, Zhejiang University, Hangzhou, China

(*Received April 13, 2020, Revised May 24, 2020, Accepted May 28, 2020*)

Abstract. A design method of a Multiple Tuned Mass Damper (MTMD) system is presented for wind induced vibration control of a cable-supported roof structure. Modal contribution analysis is carried out to determine the dominating modes of the structure for the MTMD design. Two MTMD systems are developed for two most dominating modes. Each MTMD system is composed of multiple TMDs with small masses spread at multiple locations with large responses in the corresponding mode. Frequencies of TMDs are distributed uniformly within a range around the dominating frequencies of the roof structure to enhance the robustness of the MTMD system against uncertainties of structural frequencies. Parameter optimizations are carried out by minimizing objective functions regarding the structural responses, TMD strokes, robustness and mass cost. Two optimization approaches are used: Single Objective Approach (SOA) using Sequential Quadratic Programming (SQP) with multi-start method and Multi-Objective Approach (MOA) using Non-dominated Sorting Genetic Algorithm-II (NSGA-II). The computation efficiency of the MOA is found to be superior to the SOA with consistent optimization results. A Pareto optimal front is obtained regarding the control performance and the total weight of the TMDs, from which several specific design options are proposed. The final design may be selected based on the Pareto optimal front and other engineering factors.

Keywords: multiple tuned mass dampers; vibration control; cable-supported roof; SQP with multi-start; NSGA-II

1. Introduction

Cable supported structures are widely and increasingly employed for large scale public structures, such as railroad stations, exhibition centers, gymnasiums and cable supported bridges. The flexible properties of those structures often cause serious wind induced vibration problems. Closely spaced modal frequencies and spatially complicated mode shapes are generally excited by ambient winds. The wind-induced fluctuating stress can lead to fatigue damage accumulation and result in structural failure without exceeding design wind actions (Repetto and Solari 2001). All the facts render it a significant and complicated topic to deal with the vibration control of cable supported structures. Fujino (2002) studied the wind-induced vibration control for cable-supported bridges through three aspects: Structural, aerodynamic and mechanical remedies. The control remedies for girders, pylons and cables were introduced and discussed. Cardenas *et al*. (2008) proposed a 3D nonlinear model to evaluate wind dynamic effects, damper locations and configurations for the vibration control of a real cable stayed bridge in Mexico. Zi *et al*. (2011) studied the modeling, analysis, and wind-induced vibration control of the cable-supporting system for the large spherical radio telescope.

Various control devices are extensively investigated and successfully applied to reduce excessive vibrations for cables and cable-supported structures such as viscous dampers (Zhou *et al*. 2019), tuned mass dampers (Abe and Fujino 1994, Fujino 2002, Tributsch and Adam 2012), inertial mass dampers (Lu *et al.* 2017, Wang *et al.* 2019b), eddy current dampers (Niu *et al.* 2018, Wang *et al*. 2020) and magnetorheological dampers (Duan *et al*. 2006, 2019a). The Tuned Mass Damper (TMD), as a kind of passive damper, is one of the simplest vibration control devices among them. It has many advantages, such as compactness, reliability, efficiency, low maintenance cost and free of the influence of high temperatures. However, efficiency of TMDs is highly frequency-dependent. A small offset of the tuning frequency may result in large reduction to the TMD performance. Xu and Igusa (1992) proposed a new design concept for the TMD using Multiple Tuned Mass Dampers (MTMD) with closely spaced frequencies to suppress vibration of a dynamic system. Abe and Fujino (1994) studied the characteristics and efficiency of the MTMD and found that the MTMD showed much better robustness than a conventional single TMD while maintaining more or less the same efficiency.

In recent years, the effectiveness and application of MTMD have been widely studied and verified (Elias and Matsagar 2017). Debnath *et al.* (2016) proposed an approach for simultaneous control of major horizontal, vertical and torsional modes with MTMD, and verified the approach with a MTMD system installed on a large span truss bridge. Tao *et al.* (2017) performed a parametric

*Corresponding author, Professor,
E-mail: tq1970@126.com

**Co-corresponding author, Professor,
E-mail: ceyfduan@zju.edu.cn

ISSN: 1738-1584 (Print), 1738-1991 (Online)

analysis for MTMD and found that the buffeting response of a long-span triple-tower suspension bridge can be effectively mitigated by utilizing reasonable design parameters for the MTMD system. Elias *et al.* (2017) investigated the effectiveness of the multi-mode control of a seismically excited building using distributed multiple tuned mass dampers at various floors. Wang and Shi (2019) successfully mitigated the human-induced vibration of a footbridge with a MTMD system. Wang *et al*. (2019a) found that MTMD systems demonstrated predominant and robust capacity of reducing structural vibrations under both crowd random excitations and rhythmic excitations.

With the wide application of the MTMD, optimal design for the MTMD layouts and parameters turns out to be an important subject. Warnitchai and Hoang (2006) presented a new method for the optimal MTMD design, in which a numerical optimizer was introduced to effectively handle a large number of design variables. Miguel *et al.* (2016) presented a novel robust optimization method of MTMD using the firefly algorithm to consider uncertainties in system and excitation parameters. Hussan *et al*. (2018) studied the MTMD parameter optimization with the response surface methodology and verified it for a multi-mode vibration control of wind turbine structures. Vellar *et al*. (2019) proposed a new methodology for simultaneous optimization of parameters and positions of MTMD for buildings subjected to earthquakes, and showed that the methodology considered uncertainties in the structural parameters, dynamic loads and MTMD design for MTMD robustness.

For single-objective optimization problems, Sequential Quadratic Programming (SQP) methods have been widely used owing to its robustness and high efficiency in searching for the optimum solutions (Boggs and Tolle 2000, Martí 2003, Jin *et al.* 2010, Chung *et al*. 2012). In the SQP, an optimal solution is searched by minimizing a quadratic model of the objective function subjected to the linearized constraints. Simple heuristic methods, such as multi-start methods, are usually employed together with SQP to enhance the chance of obtaining a global optimum by randomly selecting a set of starting points in the hope that one of them is close to the global optimal solution (Martí 2003, Zheng *et al*. 2006). Genetic Algorithms (GA) have also been extensively employed for various parameter optimization problems. It is a typical evolutionary algorithm using crossover and mutation operators along with random search techniques to avoid sticking in the local optimum (Holland 1975). Frans and Arfiadi (2015) proposed a hybrid coded genetic algorithm for the optimal design of MTMD, which utilized binary coded GAs to optimize the MTMD parameters and real coded GAs to optimize the location of the dampers. Chen *et al.* (2017) presented hybrid algorithms based on GA and pattern search algorithm for MTMD parameter optimization for a long span roof structure. Zahrai and Froozanfar (2019) adopted the GA for the MTMD parameter optimization to mitigate the seismic response of the Ahvaz cable-stayed bridge.

Multi-objective optimization models are usually more common and suitable for engineering practice, which involve a set of conflicting sub-objectives to be optimized.

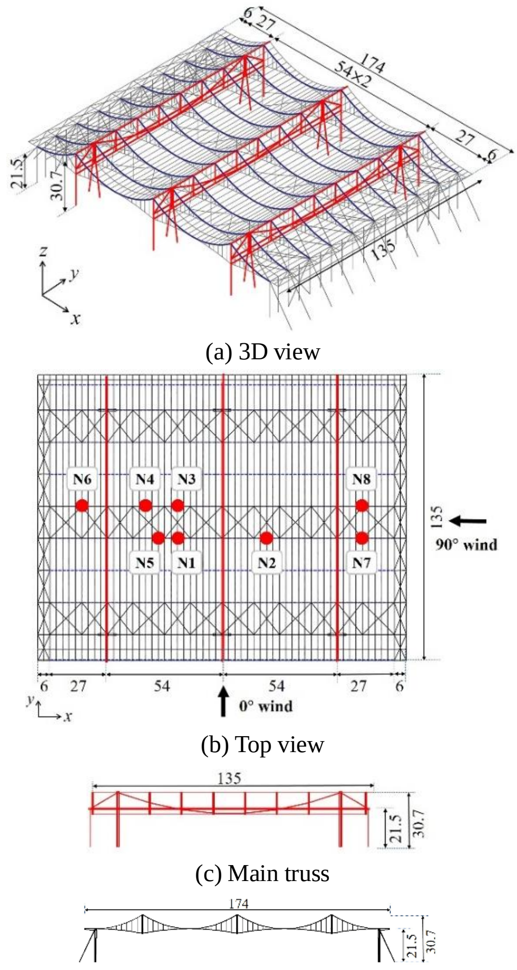

(a) 3D view

(b) Top view

(c) Main truss

(d) Cable truss

Fig. 1 A cable-supported roof structure (unit: m)

Etedali and Rakhshani (2018) employed a Multi-Objective Cuckoo Search (MOCS) method for simultaneous reduction of structural displacement responses, acceleration responses and the TMD mass ratio for a TMD parameter optimization problem. Lavan (2017) adopted the first-order multi-objective optimization approach of Izui *et al.* (2015) to simultaneously minimize structural responses, the TMD mass and the TMD stroke for a TMD design. A fast elitist Non-dominated Sorting Genetic Algorithm (NSGA-II) was developed for the multi-objective optimization by introducing the notion of non-dominated sorting in GA, aiming at finding a solution set of Pareto optimal solutions (Siinivas and Deb 1994, Deb *et al.* 2002). And it has been widely employed in engineering problems for its good performance and high computation efficiency for multi-objective problems (Jin *et al.* 2014, Kaveh *et al*. 2015, Nezami and Gholami 2016, Bagheri *et al*. 2018). Ok *et al*. (2008) employed NSGA-II for the optimal performance design of a bi-TMD system considering both the effectiveness of the bi-TMD for the original structural system and the robustness of the bi-TMD under variations in the dynamic properties of the target structure. Pourzeynali *et al.* (2013) adopted NSGA-II for the robust multi-objective optimization design of a TMD for the

Table 1 Dynamic characteristics of the cable-supported roof structure

Modes	Frequencies (Hz)	Effective modal mass (kg)			Mode shape descriptions*
		UX	UY	UZ	
1	0.447	209416	0	0	Vertical antisymmetric vibration
2	0.533	0	1841460	25	Horizontal symmetric vibration
3	0.534	527	4	0	Horizontal antisymmetric vibration
4	0.564	0	25853	2	Horizontal symmetric vibration
5	0.567	12	0	0	Horizontal antisymmetric vibration
6	0.581	105	51135	23	Horizontal antisymmetric vibration
7	0.582	2	704105	238	Horizontal symmetric vibration
8	0.631	1139	208	232056	Vertical symmetric vibration
9	0.662	628663	0	352	Vertical antisymmetric vibration (along with horizontal vibration)
10	0.689	181	2	108712	Vertical symmetric vibration
11	0.735	2458	0	171	Vertical antisymmetric vibration (along with horizontal vibration)
12	0.759	27230	0	636	Vertical antisymmetric vibration (along with horizontal vibration)
13	0.810	12	0	936	Vertical symmetric vibration
14	0.838	42	0	1367	Vertical antisymmetric vibration
15	0.853	13	92	1509880	Vertical symmetric vibration

*The main truss in the middle is regarded as the symmetric axis (Fig. 1(a))

vibration control of tall buildings. The maximum displacement, velocity and acceleration of each floor were minimized simultaneously.

In this paper, an optimal MTMD design method is presented for a cable-supported roof structure with long spans subjected to turbulent wind loads, which employs a multi-mode control of two dominating modes of the roof. Based on the previous study, the Multi-Objective Approach (MOA) is extended for the MTMD design, and a comparative study between Single Objective Approach (SOA) and MOA is performed. In Section 2, the structural characteristics, modal properties, and wind load conditions are introduced. Dynamic analysis is performed with modal superposition method for the turbulent wind loads simulated at various points on the roof by the Computational Fluid Dynamic (CFD) analysis. In Section 3, dominating modes are identified through the modal contribution analysis for the wind loads. The optimal MTMD design is achieved by two approaches. One is the SOA using the SQP with multi-start method, and the other is the MOA using the NSGA-II. Optimization results and computation efficiency of the two design approaches are compared and discussed, verifying the advantage of the MOA. An average Pareto optimal front is obtained, from which the MTMD design parameters can be determined considering additional engineering considerations, such as the control performance, TMD installation, construction procedures and cost. In Section 4, the detail control performances of four MTMD design alternatives are examined, and an additional MTMD system is proposed regarding the second dominating mode for further reduction of the roof responses, particularly on the side spans. Finally, a summary and conclusions are given in Chapter 5.

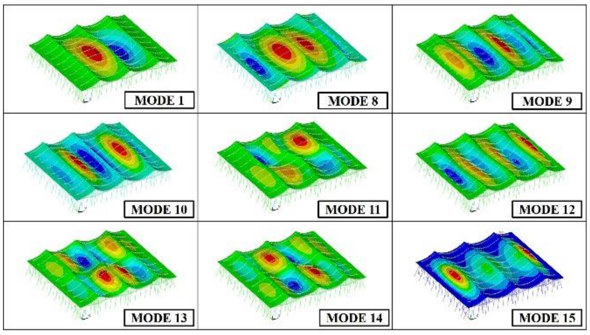

Fig. 2 Mode shapes of the roof

2. Structure description and wind load conditions

2.1 Structural characteristics

The present canvas roof structure is supported by a bi-directional cable system (Duan *et al*. 2019b). Three main steel trusses with main cables act as the main support system as shown in Figs. 1(a) and (c). Ten double-layer cable trusses act as the secondary support system as shown in Figs. 1(a) and (d). Length of the structure is 174 m, and the width is 135 m. The three main trusses divide the total length into four spans, with two middle spans of 54 m and two side spans of 27 m.

The initial balanced shape of the roof is formed by the self-weight of the roof and the pretensions of cables. Modal

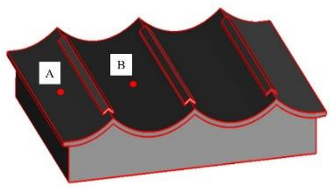

(a) 3D view of the CFD model

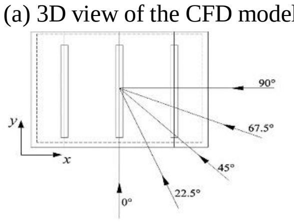

(b) Wind directions

Fig. 3 Wind load simulation

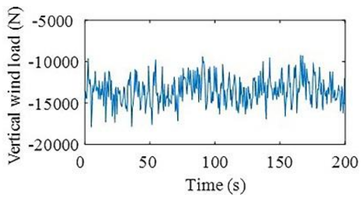

(a) 45° wind load at Node A

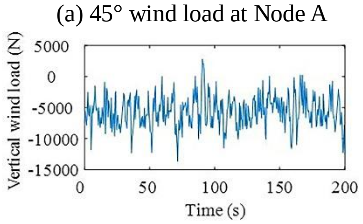

(b) 45° wind load at Node B

Fig. 4 Examples of wind load histories: Vertical components

analysis was performed, and 50 modes were extracted. Frequencies, mode shapes and effective modal mass are given for the first 15 modes in Table 1. Vertical vibration mode shapes are shown in Fig. 2. The effective modal mass in the j^{th} direction is calculated by

$$M_{eff(i,j)} = \frac{(\{\phi\}_{i,j}^{T}[M]\{1\}_j)^2}{\{\phi\}_{i,j}^{T}[M]\{\phi\}_{i,j}} \tag{1}$$

where $\{\phi\}_{i,j}$ is the mode shape vector of the i^{th} mode in the j^{th} direction; $[M]$ is the mass matrix of the structure; and $\{1\}_j$ is the load distribution vector with 1 in the j^{th} direction and zero in the other directions. The vertical effective modal masses for the vertical symmetric modes (8^{th}, 10^{th} and 15^{th}) are found to be much larger than the others in the vertical direction. Corresponding frequencies are 0.631, 0.689 and 0.853 Hz.

2.2 Wind load conditions

A CFD model was established for wind load simulation through modeling of the canvas roof and curtain walls (Fig. 3(a)) (Duan *et al*. 2019b). Wind loads with a recurrence interval of 50 years were simulated. The corresponding 10-minute wind speed is 23.76 m/s. Five wind load conditions were considered, with five wind directions, 0°, 22.5°, 45°, 67.5° and 90° (Fig. 3(b)). Wind force are provided at 590 points uniformly distributed on the roof. The duration of wind loads is 200 seconds. Nodes A and B (Fig. 3(a)) are taken as examples to show the wind load time histories obtained by the CFD analysis (Fig. 4).

Table 2 Critical nodes under 5 wind load conditions

Wind loads	0°	22.5°	45°	67.5°	90°
Critical nodes in middle spans	N1	N2	N3	N4	N5
Critical nodes in side spans	N6	N6	N6	N7	N8

Table 3 Dynamic vertical displacements ($3\sigma_k$) of critical nodes

Wind loads		0° (m)	22.5° (m)	45° (m)	67.5° (m)	90° (m)	Allowable values (m)
Middle spans	N1	0.070	0.073	0.235	0.091	0.073	0.150
	N2	0.064	0.084	0.235	0.071	0.069	
	N3	0.069	0.070	0.238	0.093	0.073	
	N4	0.057	0.055	0.167	0.117	0.073	
	N5	0.068	0.067	0.223	0.101	0.076	
Side spans	N6	0.053	0.082	0.178	0.089	0.036	0.108
	N7	0.052	0.069	0.171	0.107	0.064	
	N8	0.053	0.072	0.174	0.107	0.066	

2.3 Dynamic analysis in time domain

Two response components are involved in the wind-induced vibration: 1) the static mean component and 2) the turbulent component. The expected peak vertical displacement $\widehat{U}_k$ of the k^{th} degree-of-freedom (DOF) of the structure under the wind load is obtained as

$$\widehat{U}_k = \overline{U}_k + sign(\overline{U}_k) g \sigma_k \tag{2}$$

where $\overline{U}_k$ is the static mean response; $sign(\overline{U}_k)$ denotes the sign of $\overline{U}_k$; σ_k is the standard deviation of the vertical response; and g is a peak factor, which is taken as 3 as in the wind engineering practice.

This paper aims to reduce the dynamic responses of the roof structure. Thus, the turbulent wind-induced responses ($3\sigma_k$) are mainly taken into consideration. The first 20 modes are used for dynamic analysis using the mode superposition method. Critical nodes with the maximum dynamic vertical displacements ($3\sigma_k$) under 5 wind load conditions are determined, and the results are listed in Table 2. Locations of those nodes are shown in Fig. 1(b). The maximum responses at the critical nodes are listed in Table 3, which shows that the wind with a direction of 45° is the critical wind load condition. The corresponding critical nodes are N3 in the middle span and N6 in the side span.

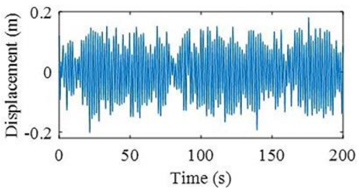

(a) Responses of N3

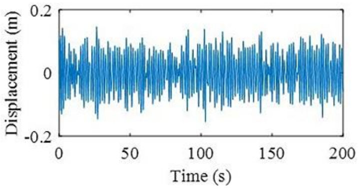

(b) Responses of N6

Fig. 5 Dynamic vertical displacement histories of N3 and N6 under 45° wind

Dynamic vertical displacement histories at N3 and N6 under 45° wind are shown in Fig. 5. The maximum dynamic responses at two nodes are found to be 0.238 and 0.178 m, which are larger than the allowable values of 0.15 and 0.108 m as described in Section 3.3.1. Therefore, a MTMD system is considered for vibration reduction of the roof in this study.

3. Optimal design of MTMD

3.1 Design procedure

The MTMD system consists of multiple small TMDs spread at multiple locations on the roof. The mass ratio μ is defined as the ratio between the total mass of the TMDs and the total mass of the roof structure $m_s = 2480000$ kg. The mass distribution factor γ is defined as the ratio of the total mass of TMDs in the middle spans to the total mass of the MTMD system. All the TMDs in the middle spans share a same mass, denoted as m_{midd}, and all the TMDs in the side spans also share a same mass, denoted as m_{side}. Then the mass of each TMD can be obtained by

$$m_{midd} = \frac{m_s \times \mu \times \gamma}{n_{midd}} \tag{3}$$

$$m_{side} = \frac{m_s \times \mu \times (1-\gamma)}{n_{side}} \tag{4}$$

where m_s is the mass of the roof structure; and n_{midd} and n_{side} are the numbers of TMDs in the middle and side spans, respectively.

The damping ratio (ξ_T) of each TMD in the MTMD system is taken as identical for simplicity. Frequencies of TMDs ($\omega_1, \ldots, \omega_n$) are distributed uniformly within a range around the corresponding frequency of the structure for the enhancement of the robustness of the MTMD system against uncertainties of structural frequencies (Abe and Fujino 1994). The non-dimensional frequency bandwidth (B) for a MTMD is defined as

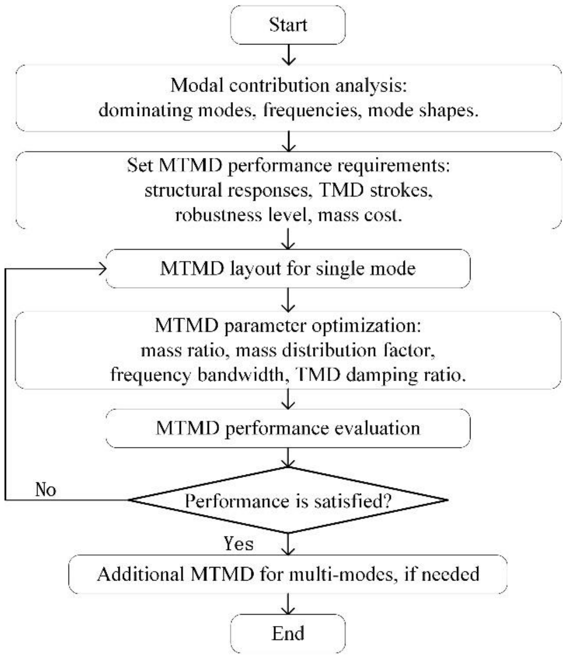

Fig. 6 MTMD design procedure

$$B = \frac{\omega_n - \omega_1}{\omega_s} \times 100\% \tag{5}$$

where ω_1 and ω_n are the lower and upper limits of TMD frequencies; and ω_s is the structural corresponding frequency of the roof.

Therefore, four parameters of the MTMD and one property of the roof structure are involved in the design of the MTMD system: μ, γ, ξ_T, B and ω_s. Determination of these values as well as the development of the whole MTMD system are going to be conducted by following the procedure shown in Fig. 6:

1. Modal contribution analysis is performed to find the mode with the largest contribution to the structural dynamic vertical displacements, which is defined as the dominating mode. The corresponding modal frequency is set as the structural dominating frequency, ω_s, and the mode shape is used to determine the MTMD layout. Details of this step are shown in Section 3.2.

2. Performance requirements for the MTMD system are set, involving the allowable dynamic vertical displacements of the roof structure, the allowable strokes of TMDs, the robustness level of the MTMD system and the limit of the mass cost.

3. MTMD parameters are optimized with the consideration of the structural response reduction, TMD strokes, system robustness as well as the total mass closely related to the cost. Two methods are used for the parameter optimization. They are the SQP with multi-start (Boggs and Tolle 2000, Martí 2003) and the NSGA-II (Deb *et al*. 2002) as in Section 3.3.

4. Finally, the MTMD system is developed and the system performance is verified (Section 4.1). If the structural vibration shall be mitigated further, additional MTMD systems may be considered for multi-mode control (Section 4.2).

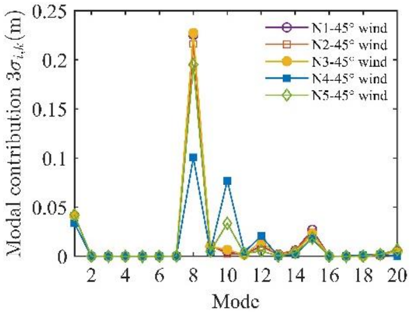

(a) N1-N5 on the middle spans

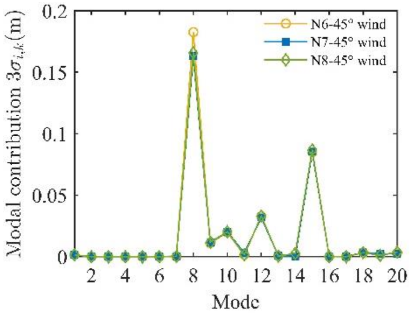

(b) N6-N8 on the side spans

Fig. 7 Modal contribution analysis for N1-N8

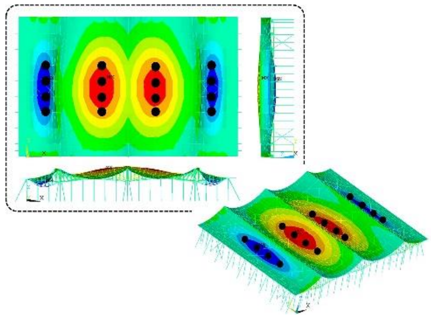

Fig. 8 Mode shape of the 8th mode

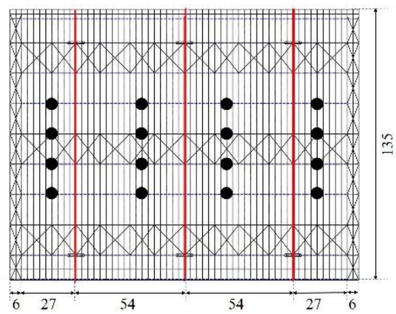

Fig. 9 MTMD initial layout

3.2 Dominating modes and MTMD layout

Dynamic response of the k^{th} DOF in a N degrees-of-freedom structure can be computed effectively using the modal superposition method

$$U_k(\mathrm{t}) = \sum_{i=1}^{l} U_{i,k}(\mathrm{t}) = \sum_{i=1}^{l} \phi_{i,k} q_i(t) \quad (l \ll N) \tag{6}$$

where $U_{i,k}(\mathrm{t})$ is the modal response time history of the k^{th} DOF associated with the i^{th} mode; $\phi_{i,k}$ is the modal displacement of the k^{th} DOF of the i^{th} mode; $q_i(t)$ is the modal coordinate of the i^{th} mode; and l is the number of modes considered in the dynamic analysis.

Similar to Eq. (2), the peak value of the modal response $\widehat{U}_{i,k}$ is defined as

$$\widehat{U}_{i,k} = \overline{U}_{i,k} + sign(\overline{U}_{i,k}) g\sigma_{i,k} \tag{7}$$

where $\overline{U}_{i,k}$ is the static mean modal contribution; $sign(\overline{U}_{i,k}) g\sigma_{i,k}$ is the turbulent modal contribution; and g is taken as 3.

In this paper, the mode with the largest turbulent modal contribution to the dynamic responses at the most critical nodes (N3 and N6) under the critical wind load condition (45° wind) is taken as the *dominating mode*. Modal contribution analysis was performed for all the critical nodes (N1-N8) under 45° wind load using the first 20 modes. Results in Fig. 7 show that the modal contribution of the 8th mode, which is a vertical symmetric mode (Table 1), is the most predominant among the 20 modes for the dynamic responses of all the critical nodes. The 10th and 15th modes are also important to the nodes in the middle spans (N1-N5). On the other hand, the 10th, 12th and 15th modes also provide significant contribution to the nodes in the side spans (N6-N8). The mode shape of the 8th mode is shown in Fig. 8, and its frequency is 0.631 Hz as in Table 1. Accordingly, the initial MTMD layout is taken considering the points of the peak responses of the 8th mode shape, which results in 16 TMDs distributed in the middle and side spans (Figs. 8-9).

3.3 Parameter optimization method

3.3.1 Performance indices

Five requirements are set for the MTMD system in this study: 1) the ratio of dynamic deflection of the roof to the span length is less than a prescribed value considering the structural safety; 2) large visible motion of the roof is prevented to avoid the anxiety of people inside the building; 3) the strokes of TMDs are within an allowable value considering the installation space; 4) the robustness of the MTMD system is guaranteed against the uncertainty in the structural characteristics; and 5) the total mass of the MTMD system is limited to a prescribed value for an economic design. Considering all the above requirements, five performance indices are proposed for the MTMD design.

The performance indices for dynamic responses of the roof in the middle and side spans and TMDs are

$$R_{midd} = \frac{z_{max}^{midd}}{z_{allow}^{midd}} \tag{8}$$

$$R_{side} = \frac{z_{max}^{side}}{z_{allow}^{side}} \tag{9}$$

$$R_{tmd} = \frac{z_{max}^{tmd}}{z_{allow}^{tmd}} \tag{10}$$

where z_{max}^{midd}, z_{max}^{side} and z_{max}^{tmd} are the maximum dynamic vertical displacements in middle spans, side spans and TMDs; and z_{allow}^{midd}, z_{allow}^{side} and z_{allow}^{tmd} are the allowable values of those displacements. z_{allow}^{midd} and z_{allow}^{side} are defined considering the allowable ratio of the dynamic deflection to the span length, 1/250 (Duan *et al*. 2019b), and the prescribed allowable visible dynamic deflection of the roof which is taken as 0.15 m

$$z_{allow}^{k} = \min\left\{\frac{l_k}{250}, 0.15\, m\right\}, \qquad \mathrm{k = midd, side} \tag{11}$$

where l_k is the length of the k^{th} span ($k = midd,\ side$). z_{allow}^{midd} and z_{allow}^{side} are obtained as 0.15 m and 0.108 m, and z_{allow}^{tmd} is taken as 1.0 m in this study.

Robustness of a MTMD design is defined as

$$R_{robust} = \frac{r}{r_{allow}} \tag{12}$$

where r is the robustness coefficient of the MTMD design; and r_{allow} is the allowable value. The robustness is evaluated by comparing the structural response reduction rates under different structural states with two modified values of pretensions in the cables as

$$r = \frac{1}{2}\left(\left|\frac{rr'_{midd} - rr_{midd}}{rr_{midd}}\right| + \left|\frac{rr'_{side} - rr_{side}}{rr_{side}}\right|\right) \tag{13}$$

where rr_{midd} and rr_{side} are the response reduction rates of the maximum dynamic displacements in the middle and side spans with the initial cable pretension; rr'_{midd} and rr'_{side} are the response reduction rates with two modified cable pretensions to 80% and 110%. The corresponding frequency shifts in the first 20 modes are 3-10% and 2-5% under the two pretensions, respectively.

The response reduction rate for a MTMD design is calculated by

$$rr_k = \frac{z_{max,0}^{k} - z_{max}^{k}}{z_{max,0}^{k}} \times 100\% \quad (k = midd, side) \tag{14}$$

where z_{max}^{k} and $z_{max,0}^{k}$ are the maximum dynamic displacements at the k^{th} span ($k = midd, side$) with and without the MTMD. The allowable value of the robustness index r_{allow} is taken as 35%.

Table 4 Range of optimization parameters

Parameters	Range	Interval
μ	0.001 - 0.020	0.001
γ	0 - 1.0	0.1
B	0.05 - 0.20	0.05
ξ_T	0.01 - 0.20	0.02

Another performance index for the MTMD cost is introduced considering the MTMD mass ratio as

$$R_{mass} = \frac{\mu}{\mu_{allow}} \tag{15}$$

where μ is the mass ratio between the total TMD mass and the mass of the roof structure; m_s= 2480000 kg; and μ_{allow} is the allowable ratio which is taken as 0.02.

3.3.2 Single objective approach (SOA)

Five objectives are involved in the parameter optimization to minimize the five performance indices introduced in 3.3.1. A common difficulty with the multi-objective optimization is the appearance of objective conflicts – none of the feasible solutions allow simultaneous optimal solutions for all objectives (Siinivas and Deb 1994). The method of objective weighting is one of the classical techniques to solve such problems by combining multiple objectives with prescribed weights into a single objective function. Then the controlled variables are optimized through the minimization or maximization of the formulated objective function.

The five objectives are divided into two groups: one for structural control performance (R_{midd}, R_{side}, R_{tmd} and R_{robust}) and the other for the MTMD cost (R_{mass}). In this study, instead of one optimal MTMD design considering the control performance and MTMD cost simultaneously, a set of design options for various MTMD cost and the corresponding control performance are selected for the final decision making. Thus, an objective function for MTMD performance was formulated as

$$\begin{aligned} &\min J(x) = \min\,(w_1 R_{midd}(x) + w_2 R_{side}(x) \\ &\qquad\qquad + w_3 R_{tmd}(x) + w_4 R_{robust}(x)) \\ &s.t. \\ &x = \{\mu, \gamma, B, \xi_T\}^T \\ &R_{midd} \le\ 1,\ R_{side} \le\ 1,\ \ R_{tmd} \le 1,\ \ R_{robust} \le 1 \end{aligned} \tag{16}$$

where x is the MTMD parameter vector, in which μ is the mass ratio of the MTMD system; γ is the mass distribution factor; B is the non-dimensional frequency bandwidth of the MTMD; and ξ_T is the damping ratio of each TMD; and w_1, w_2, w_3 and w_4 are the prescribed weight factors for the performance indices.

In this study, SQP algorithm is adopted for the optimization procedure (Boggs and Tolle 2000, Chung *et al*. 2012). To search for the global minimum, the function *MultiStart*, which is provided by MATLAB Optimization Toolbox, was used with 100 start points uniformly distributed within the bounds using the *fmincon* ‘SQP’ algorithm (Martí 2003, MathWorks 2020).

Parameter optimization was carried out for the single objective function related to the control performance as in Eq. (16) for a set of the prescribed MTMD costs (R_{mass}). At first a dataset was constructed for the dynamic responses of the structure-MTMD system by carrying out dynamic analyses for various combinations of the control parameters. The ranges and intervals of the parameters for dynamic analysis are shown in Table 4. In the optimization process,

Table 5 Weights for $J(\boldsymbol{x})$

No.	Weight settings
w^1	(0.25, 0.25, 0.25, 0.25)
w^2	(0.28, 0.28, 0.21, 0.25)
w^3	(0.28, 0.28, 0.23, 0.23)
w^4	(0.28, 0.28, 0.25, 0.21)
w^5	(0.30, 0.30, 0.15, 0.25)
w^6	(0.30, 0.30, 0.20, 0.20)
w^7	(0.30, 0.30, 0.22, 0.18)
w^8	(0.30, 0.30, 0.25, 0.15)
w^9	(0.30, 0.30, 0.27, 0.13)
w^{10}	(0.35, 0.35, 0.15, 0.15)
w^{11}	(0.35, 0.35, 0.20, 0.10)

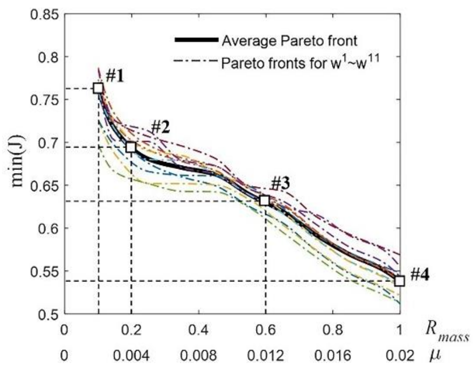

Fig. 10 Pareto fronts for $w^1 - w^{11}$ by SOA

the computation of the performance indices and their gradients were carried out using interpolation of the pre-computed values for the parameters in Table 4 for the computational efficiency.

Eleven sets of weights for the performance indices in Eq. (16) were selected based on the reasoning that the weights for the roof responses shall be larger than those for the MTMD response and control robustness as shown in Table 5. For each weight set, optimization was performed for twenty mass ratios, from 0.001 to 0.020 with an interval of 0.001, and the relationship between the MTMD cost (R_{mass}) and the corresponding optimum performance were obtained as the Pareto front. Fig. 10 shows 11 Pareto optimal fronts, from which the average Pareto optimal front is obtained for the optimal MTMD design option considering the ambiguity of the weight selection. During the optimization process, it was found that when the mass ratio was equal to 0.001, no feasible solution existed.

Fig. 10 shows that the control performance gets improved with the increase of the MTMD (mass) cost. The MTMD parameters shall be determined considering the trade-off between the control performance and MTMD cost along the average Pareto front. The maximum bend angle (Hansen and Oleary 1993) appears near the point with a $\mu = 0.004$. At the left of this point, the control performance (J in Eq. (16)) improves sharply with the increase of μ. After this point, the gradient of the curve becomes smaller indicating a relative lower efficiency of the MTMD (mass) cost. Therefore, the design parameter combination with a mass ratio of 0.004 appears to be the most economical, although the final decision may be made considering the additional engineering factors by the decision maker. Four optimal design alternatives with μ of 0.002, 0.004, 0.012, and 0.02 are presented and discussed in detail in Section 4.1.

3.3.3 Multi-objective approach (MOA)

MOA is employed in the optimal design of MTMD to investigate the effect of the weights more rigorously and also to verify the optimal solutions from the SOA given in Section 3.3.2. The MOA with five objective functions is defined as

$$\begin{aligned} &\min\,[R_{midd}(x), R_{side}(x), R_{tmd}(x), R_{robust}(x), R_{mass}(x)] \\ &s.t. \\ &x = (\mu, \gamma, B, \xi_T)^T \\ &R_{midd} \leq 1,\ R_{side} \leq 1,\ R_{tmd} \leq 1,\ R_{robust} \leq 1,\ R_{mass} \leq 1 \end{aligned} \tag{17}$$

where the ranges of the control parameters are same to the SOA cases shown in Table 4.

The non-dominated sorting genetic algorithm is used to obtain the Pareto-optimal solutions (Siinivas and Deb 1994) in this study. More specifically, the fast elitist NSGA-II is employed to reduce the computational complexity of the NSGA by introducing a fast non-dominated sorting approach (Deb *et al.* 2002). In the NSGA-II, the parent population of size $2N$ is sorted based on the non-domination. Each solution is assigned a non-domination Rank (1 is the best rank) and a crowd distance (Cd) measuring the density of solutions in the neighborhood. Tournament selection, recombination, and mutation operators are carried out to create a child population of size *N*. Then the parent and child population are combined and sorted, and the individuals with lower Rank and larger Cd within the combined population are selected to form the parent population for the next generation (Deb *et al*. 2002).

In this study, the size of the parent population is taken as $2N = 1000$, and the maximum generation is $G = 1000$. A list of alternative solutions sorted with Rank and Cd is obtained in the final generation. Ten of the non-dominated solutions in the order of Cd are shown in Table 6. Obviously, the sequence of solutions sorted with Rank and Cd may be different from the sequence of preference in engineering practice. Although the non-dominated optimal solutions with respect to five objectives were obtained, it is still difficult to select proper MTMD parameters among hundreds of Pareto solutions. Therefore, the MOA solutions in a 5-dimensinoal space of objective functions are projected into a 2-dimensional sub-space consisting of the weighted control performance (J in Eq. (16)) and the MTMD cost (R_{mass}) for each of eleven sets of the weights listed in Table 5 as in the SOA. For a weight set (w^1), the optimal solutions and the Pareto optimal front in the $J - R_{mass}$ space are shown in Fig. 11, which results in a very consistent Pareto front to the one by the SOA, although several solutions are not captured. Similarly to the SOA, the average Pareto optimal front is obtained by combining the

Table 1 Dynamic characteristics of the cable-supported roof structure

No.	μ	γ	B	ξ_T	z_{max}^{midd} (m)	z_{max}^{side} (m)	z_{max}^{tmd} (m)	r (%)	Rank	Cd*
1	0.02	0.9	0.20	0.19	0.095	0.077	0.500	19	1	Inf
2	0.013	0.6	0.05	0.07	0.147	0.108	0.720	8	1	Inf
3	0.014	0.3	0.05	0.11	0.131	0.106	0.472	9	1	0.116
4	0.012	0.0	0.18	0.11	0.138	0.065	0.390	35	1	0.092
5	0.011	0.3	0.20	0.17	0.109	0.090	0.689	12	1	0.090
6	0.012	0.1	0.05	0.18	0.137	0.090	0.370	21	1	0.089
7	0.008	1.0	0.05	0.17	0.125	0.099	0.598	16	1	0.088
8	0.013	0.3	0.20	0.18	0.105	0.084	0.610	18	1	0.080
9	0.002	0.8	0.17	0.12	0.111	0.089	0.880	29	1	0.069
10	0.004	0.0	0.20	0.14	0.125	0.076	0.570	30	1	0.066

* Crowd distance of boundary points within a non-domination front is denoted as 'Inf' (Deb *et al.* 2002)

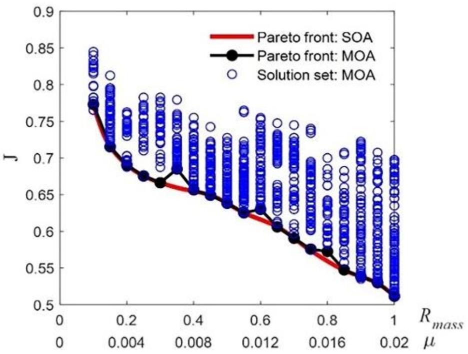

Fig. 11 $J(\boldsymbol{x})$ vs R_{mass} for w^1

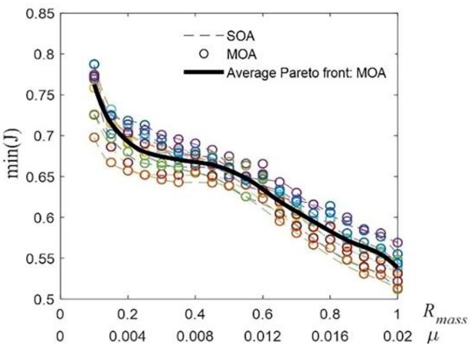

Fig. 12 Pareto fronts for $w^1 - w^{11}$ by MOA

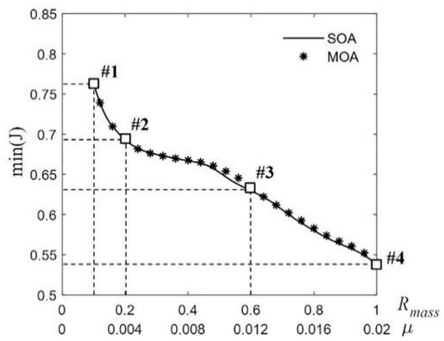

Fig. 13 Comparison of average Pareto fronts by SOA and MOA

results for eleven different sets of weights as in Fig. 12. The averaging operations eliminate the influence of solutions that are not captured in MOA. Thus, the average Pareto optimal front is found to be in excellent agreement with the one from the SOA as in Fig. 13, which verifies the consistency in the optimization solutions by two approaches. As in the SOA, four MTMD design alternatives (#1 - #4 in Fig. 13) are selected based on the average Pareto optimal front for further investigation of the control performance in detail. They are the cases corresponding to four different values of the MTMD mass ratios (μ) as 0.002, 0.004, 0.012 and 0.02.

The computation time of MOA and SOA are 860 s and 13290 s, respectively. In MOA, after the non-dominated solution set is obtained by NSGA-II with N = 500 and G = 1000, the objective function J for eleven weight sets can be easily computed by linear combinations of the performance indices for the 1000 non-dominated solutions. However, in SOA, the SQP integrated with multi-start algorithm using 100 start points shall be carried out repeatedly for eleven weight sets, and the computation time is about 1200 s for each weight set. The computational efficiency of the MOA using NSGA-II is expected to be more apparent compared with the SOA using the SQP with multi-start, as the number of the objective functions increases.

4. MTMD system and performance

The control performances on the roof responses are investigated for four MTMD design alternatives (MTMD1: #1 - #4 in Fig. 13) developed mainly for the 8th mode of the roof structure in the vertical direction as in Section 3. Then an additional MTMD system (MTMD2) is introduced for the 15th mode for the further improvement in the control performance.

4.1 Single-mode control with MTMD1

As discussed in Sections 3.3.2 and 3.3.3, four design alternatives for MTMD1 shown in Fig. 13 were selected based on the shape of the average Pareto optimal front.

Table 7 Design alternatives and control performance of MTMD1

No.	μ	γ	B	ξ_T	z_{max}^{midd} (m)	z_{max}^{side} (m)	z_{max}^{tmd} (m)	r (%)
#1	0.002	1.0	0.20	0.11	0.116	0.095	0.921	19
#2	0.004	0.3	0.20	0.19	0.106	0.075	0.723	22
#3	0.012	0.3	0.20	0.11	0.114	0.066	0.431	23
#4	0.020	0.9	0.10	0.18	0.103	0.071	0.213	17
Max. allowable	0.020	1.0	0.20	0.20	0.150	0.108	1.000	35

Table 8 Dynamic vertical displacements (3σ) of critical nodes

Design options	N1 (m)	N2 (m)	N3 (m)	N4 (m)	N5 (m)	N6 (m)	N7 (m)	N8 (m)
w/o MTMD	0.235	0.235	0.238	0.167	0.223	0.178	0.171	0.174
#1 ($\mu = 0.002$)	0.099	0.111	0.103	0.110	0.110	0.092	0.093	0.095
#2 ($\mu = 0.004$)	0.082	0.083	0.085	0.090	0.088	0.075	0.065	0.067
#3 ($\mu = 0.012$)	0.089	0.093	0.092	0.097	0.098	0.065	0.057	0.059
#4 ($\mu = 0.020$)	0.079	0.077	0.081	0.093	0.086	0.070	0.063	0.065
Max. allowable			0.150				0.108	

Table 9 Reduction rates of dynamic vertical displacements of critical nodes

Design options	N1 (%)	N2 (%)	N3 (%)	N4 (%)	N5 (%)	N6 (%)	N7 (%)	N8 (%)
#1 ($\mu = 0.002$)	58	53	57	34	51	48	45	45
#2 ($\mu = 0.004$)	65	65	64	46	61	58	62	62
#3 ($\mu = 0.012$)	62	60	62	42	56	63	67	66
#4 ($\mu = 0.020$)	66	67	66	45	61	61	63	63

Table 10 Reduction rates of dynamic vertical displacements under 80% cable pretensions

Design options	N1 (%)	N2 (%)	N3 (%)	N4 (%)	N5 (%)	N6 (%)	N7 (%)	N8 (%)
#1 ($\mu = 0.002$)	46(-12)	47(-6)	46(-11)	29(-5)	34(-17)	39(-9)	39(-7)	38(-7)
#2 ($\mu = 0.004$)	51(-14)	54(-11)	51(-13)	57(+10)	46(-15)	47(-11)	47(-16)	46(-16)
#3 ($\mu = 0.012$)	50(-12)	52(-8)	50(-12)	50(+8)	41(-15)	37(-26)	51(-15)	51(-15)
#4 ($\mu = 0.020$)	48(-18)	49(-18)	48(-18)	55(+10)	48(-13)	44(-16)	51(-12)	50(-12)

Table 11 Reduction rates of dynamic vertical displacements under 110% cable pretensions

Design options	N1 (%)	N2 (%)	N3 (%)	N4 (%)	N5 (%)	N6 (%)	N7 (%)	N8 (%)
#1 ($\mu = 0.002$)	44(-14)	43(-9)	43(-14)	28(-7)	38(-12)	32(-16)	32(-14)	32(-14)
#2 ($\mu = 0.004$)	52(-13)	52(-12)	51(-13)	27(-19)	45(-15)	44(-14)	50(-12)	49(-12)
#3 ($\mu = 0.012$)	46(-16)	48(-12)	46(-16)	32(-9)	40(-17)	52(-11)	57(-9)	56(-10)
#4 ($\mu = 0.020$)	49(-17)	50(-17)	48(-18)	43(-2)	51(-10)	52(-9)	47(-16)	50(-13)

MTMD1 parameters and their control performance are shown in Table 7. The layout of MTMD1 is shown in Fig. 9. Performance on the detail roof responses are investigated for four design options in this section.

I. Dynamic displacements at critical nodes: The dynamic vertical displacements (3σ) and reduction rates at critical nodes (N1, …, N8) are calculated under 45° wind for each of four MTMD1 design options and the results are shown in Tables 8-9. It can be found that dynamic responses are smaller than the allowable values at all nodes after introducing any of the design options. The response reduction rates are in the range of 34-67%. Apparent enhancement can be found in the response reduction rates, when the MTMD1 mass ratio (μ) increases from 0.002 to 0.004 (i.e., from Options 1 to 2). However, with the increase of the mass ratio from 0.004 to 0.020 (i.e., from Options 2 to 4), improvements of the response reduction rates between two options are arbitrary and small,

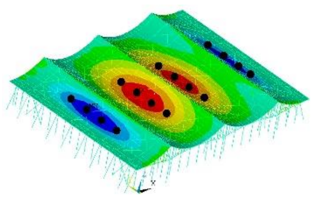

(a) MTMD1: 8th mode

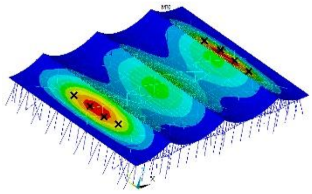

(b) MTMD2: 15th mode

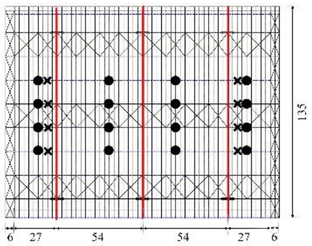

(c) MTMD layouts

Fig. 14 MTMD layout for multi-mode control design

Table 12 MTMD parameters for multi-mode control system

Design options	MTMD1				MTMD2			
	μ^1	γ^1	B^1	ξ_T^1	μ^2	γ^2	B^2	ξ_T^2
#1	0.002	1	0.2	0.11	0.001	0	0.10	0.17
#2	0.004	0.3	0.2	0.19	0.001	0	0.05	0.19
#3	0.012	0.3	0.2	0.11	0.001	0	0.20	0.18
#4	0.02	0.9	0.1	0.18	0.001	0	0.15	0.19

Table 13 Optimal MTMD systems: Masses, layouts, and frequencies of TMDs

Design options	MTMD1 (ω_{TMD1} = 0.631 Hz)		MTMD2 (ω_{TMD2} = 0.835 Hz)
	Middle spans	Side spans	Side spans
#1 (μ = 0.003)	8 @ 620 kg	----*	8 @ 310 kg
#2 (μ = 0.005)	8 @ 372 kg	8 @ 868 kg	8 @ 310 kg
#3 (μ = 0.013)	8 @ 1116 kg	8 @ 2604 kg	8 @ 310 kg
#4 (μ = 0.021)	8 @ 5580 kg	8 @ 620 kg	8 @ 310 kg

*Notes: All TMDs of MTMD1 in Option 1 are allocated to the middle spans. ω_{TMD1} and ω_{TMD2} are central frequencies among TMDs in MTMD1 and MTMD2. Locations of TMDs are shown in Fig. 14.

as discussed similarly based on the average Pareto optimal front in Fig. 10. Therefore, Option 2 with the mass ratio of

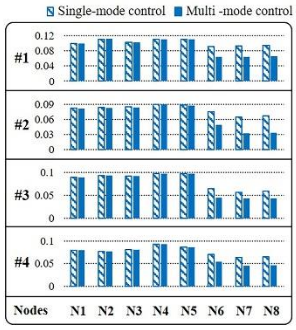

Fig. 15 Dynamic vertical displacements (m) at critical nodes for several design options

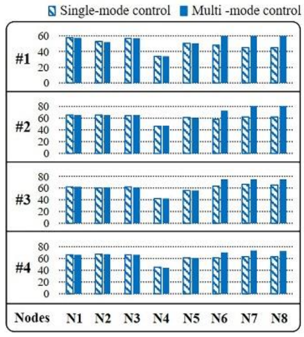

Fig. 16 Reduction rates (%) of dynamic vertical displacements of critical nodes for several design options

0.004 can be selected as the best solution of MTMD1 for the structural response mitigation.

II. TMD strokes: The maximum dynamic strokes of TMDs are found as 0.921, 0.723, 0.431 and 0.213 m for four MTMD1 designs, which are smaller than the allowable value of 1.0 m. The results also indicate that the increase of the mass ratio leads to better performance on the TMD stroke. The static elongation of all TMDs are consistently 0.624 m, because the TMD stiffness increases proportionally to the TMD mass.

III. Robustness: Variations of the structural characteristics are simulated by changes in the pretensions of cables. Two structural states are considered: one with 80% of the initial pretensions in cables, and the other with 110% of the initial pretensions. The response reduction rates at critical nodes under the two structural states are shown in Tables 10-11. Values in parentheses are the differences in the reduction rates from those of the initial structural state. The maximum difference is found as 19%. However, the response reduction rates still remain as high as 27-57% under the variations of the pretensions, while the reduction rates were in the range of 34-67% for the original structure.

4.2 Muti-mode control with MTMD1 and MTMD2

MTMD1 developed in Section 4.1 is for the 8th mode. New MTMD2 is designed for further mitigation of the roof responses on the side spans, of which the maximum response is fairly close to the allowable value of 0.108 m

Table 14 Reduction rates of dynamic vertical displacements under 80% cable pretensions

Design options	N1 (%)	N2 (%)	N3 (%)	N4 (%)	N5 (%)	N6 (%)	N7 (%)	N8 (%)
#1 ($\mu = 0.003$)	46(-12)	47(-5)	46(-11)	32(-2)	35(-16)	52(-12)	52(-9)	53(-8)
#2 ($\mu = 0.005$)	47(-18)	53(-12)	46(-19)	58(+11)	43(-18)	62(-11)	62(-20)	61(-20)
#3 ($\mu = 0.013$)	49(-13)	53(-8)	49(-12)	50(+8)	40(-16)	61(-14)	61(-14)	60(-15)
#4 ($\mu = 0.021$)	48(-18)	49(-18)	47(-19)	55(+11)	47(-14)	53(-17)	65(-9)	64(-10)

Table 15 Reduction rates of dynamic vertical displacements under 110% cable pretensions

Design options	N1 (%)	N2 (%)	N3 (%)	N4 (%)	N5 (%)	N6 (%)	N7 (%)	N8 (%)
#1 ($\mu = 0.003$)	44(-14)	43(-9)	43(-14)	28(-6)	38(-12)	57(-7)	61(-1)	62(+1)
#2 ($\mu = 0.005$)	52(-14)	52(-13)	51(-14)	28(-19)	46(-15)	64(-8)	73(-8)	74(-6)
#3 ($\mu = 0.013$)	47(-15)	48(-12)	47(-15)	33(-9)	40(-16)	69(-6)	67(-7)	68(-7)
#4 ($\mu = 0.021$)	51(-15)	50(-17)	50(-16)	44(-0)	54(-8)	66(-3)	65(-8)	72(-1)

particularly for Design Option 1 as shown in Table 8. In this study, the advantage of multi-mode control over single-mode control method is explored. The 15^{th} mode was determined as the dominating mode based on the modal shape and the modal contribution to the nodes (N6-N8) on the side spans shown in Figs. 2 and 7(b). The 8^{th} and 15^{th} mode shapes with MTMD layout for the multi-mode control design are shown in Fig. 14.

Optimal MTMD design is developed for each of four MTMD1 design options obtained in Section 4.1, while the mass ratio of MTMD2 is fixed as 0.001. The optimal solutions are shown in Table 12. The corresponding properties of the four MTMD design are shown in Table 13. The detail performance of those four multi-mode control designs are examined as follows.

I. Dynamic displacements of critical nodes: Dynamic vertical displacements (3σ) and response reduction rates at critical nodes (N1, …, N8) were evaluated under 45° wind. Figs. 15-16 show that the roof responses on the side spans (N6-N8) reduce significantly compared with the results with only MTMD1. On the other hand, the responses on the middle spans remain almost the same. The maximum additional reductions of the side span responses are found to be 17, 19, 12 and 11% with four MTMD2 design options, which indicates a considerable improvement by adding MTMD2 with a small mass ratio of 0.001. Consequently, the multi-mode control options tend to provide close or even better performance on structural response reduction with smaller mass ratios compared with single-mode control options as shown in Fig. 16. For example, the multi-mode control option #2 (total $\mu = 0.005$ in Table 13) gives larger response reduction rates in side spans and similar response reduction rates in middle spans compared with the single-mode control option #3 ($\mu = 0.012$ in Table 7). Thus, the multi-mode control options are preferred in this study for their higher efficiency in the MTMD mass and cost.

II. TMD strokes: The maximum dynamic strokes of TMDs are 0.916, 0.700, 0.410 and 0.216 m with the four additional MTMD2 design options, which are practically unchanged from those with MTMD1 only. The static elongations of TMDs are 0.624 and 0.329 m for MTMD1 and MTMD2, respectively.

III. Robustness: The response reduction rates at critical nodes are examined under two varied structural states with 80 and 110% cable pretensions, and the results are showed in Tables 14-15. Through comparison with the results with only MTMD1 in Tables 10-11, it can be observed that the addition of MTMD2 results in significant improvements in the robustness of the nodal displacements on the side spans, while it causes little changes to the nodes on the middle spans.

Four optimal design options for MTMD have been proposed and investigated for the multi-mode control system. Option 2 with mass ratios of 0.004 for MTMD1 and 0.001 for MTMD2 seems to be the best solution for structural response mitigation with good control performance with low cost. However, its maximum TMD stroke is rather high (0.70 m), thus Option 3 with a smaller TMD stroke (0.41 m) but with a higher mass ratio (0.012 and 0.001) can be also a reasonable candidate. All of four design options exhibit similar satisfactory robustness. The final design may be determined based on the results of the Pareto optimal front and other engineering factors such as project budget, TMD installation, and construction procedures.

5. Conclusions

An optimal design method for a MTMD system is presented for wind induced vibration reduction of a large-scale cable-supported roof structure. Main procedures and conclusions of the study are summarized as follows:

1. Two dominating modes of the roof structure were identified as the 8^{th} and 15^{th} modes through the modal contribution analysis for the wind loads. Accordingly, a multi-mode MTMD system was developed consisting of two sub-systems (MTMD1 and MTMD2), which were tuned to those frequencies.

2. Multiple objective functions are introduced for MTMD design regarding the structural responses, TMD

strokes, robustness, and mass cost. Two optimization approaches are used for the MTMD parameters: single objective approach using SQP with Multi-start, and multi-objective approach using NSGA-II. A Pareto front was obtained regarding MTMD performance and cost for decision making. The computation efficiency of the MOA is found to be superior to the SOA requiring repeated computations for many sets of weights on the multiple performance indices.

3. Four design options with different mass ratios were selected and their control performance were analyzed. The best option is found as a system consisting of MTMD1 and MTMD2 with mass ratios of 0.004 and 0.001. The corresponding structural response reduction rates are as high as 65% and 81% on the middle and side spans. The maximum TMD stroke is found as 0.70 m, thus another design option with the higher mass ratios (0.012 and 0.001 for MTMD1 and MTMD2) may be considered as an alternative to reduce the TMD stroke to 0.41 m. The control performance is found to be very robust against the uncertainty in the modal properties of the roof structure owing to the frequency bandwidth introduced in the MTMD design.

4. The final MTMD design may be determined based on the results of the Pareto optimal front with other engineering considerations, such as available budget, MTMD installation, and construction procedures.

Acknowledgments

This research work was supported by the National Key R&D Program of China (2018YFE0125400, 2017YFC0806100, and 2019YFE0112600) and the National Natural Science Foundation of China (U1709216, 51578419, 51522811, 51478429, and 90915008).

References

Abe, M. and Fujino, Y. (1994), "Dynamic characterization of multiple tuned mass dampers and some design formulas", *Earthq. Eng. Struct. Dyn.*, **23**(8), 813-835. https://doi.org/10.1002/eqe.4290230802.

Bagheri, M.R., Mosayebi, M., Mandian, A. and Keshavarzi, A. (2018), "Weighted sum Pareto optimization of a three dimensional passenger vehicle suspension model using NSGA-II for ride comfort and ride safety", *Smart Struct. Syst., Int. J.*, **22**(4), 469-479. https://doi.org/10.12989/sss.2018.22.4.469.

Boggs, P.T. and Tolle, J.W. (2000), "Sequential quadratic programming for large-scale nonlinear optimization", *J. Comput. Appl. Math.*, **124**(1-2), 123-137. https://doi.org/10.1016/S0377-0427(00)00429-5.

Cardenas, R.A., Viramontes, F.J.C., Gonzalez, A.D. and Ruiz, G.H. (2008), "Analysis for the optimal location of cable damping systems on stayed bridges", *Nonlinear Dyn.*, **52**(4), 347-359. https://doi.org/10.1007/s11071-007-9283-5.

Chen, X., Li, A.Q., Zhang, Z.Q., Zhou, G.D. and Cao, L.L. (2017), "Optimization design of MTMD for vibration comfort control of long-span roof structure", *J. Vib. Eng.*, **2017**(5), 827-836. https://doi.org/10.16385/j.cnki.issn.1004-4523.2017.05.016.

Chung, T.T., Cho, S., Yun, C.B. and Sohn, H. (2012), "Finite element model updating of Canton Tower using regularization technique", *Smart Struct. Syst., Int. J.*, **10**(4-5), 459-470. https://doi.org/10.12989/sss.2012.10.4_5.459.

Deb, K., Pratap, A., Agarwal, S. and Meyarivan, T. (2002), "A fast and elitist multiobjective genetic algorithm: NSGA-II", *IEEE Trans. Evol. Comput.*, **6**(2), 182-197. https://doi.org/10.1109/4235.996017.

Debnath, N., Dutta, A. and Deb, S.K. (2016), "Multi-modal passive-vibration control of bridges under general loading-condition", *Procedia Eng.*, **144**, 264-273. https://doi.org/10.1016/j.proeng.2016.05.132.

Duan, Y.F., Ni, Y.Q. and Ko, J.M. (2006), "Cable vibration control using magnetorheological dampers", *J. Intell. Mater. Syst. Struct.*, **17**(4), 321-325. https://doi.org/10.1142/9789812702197_0121.

Duan, Y.F., Ni, Y.Q., Zhang, H.M., Spencer, B.F., Ko, J.M. and Dong, S.H. (2019a), "Design formulas for vibration control of sagged cables using passive MR dampers", *Smart Struct. Syst., Int. J.*, **23**(6), 537-551. https://doi.org/10.12989/sss.2019.23.6.537.

Duan, Y.F., Wang, X.C., Dong, S.H. and Teng, Q. (2019b), "Technical report on wind-induced vibration analysis and vibration control for the Shijiazhuang international exhibition center", College of Civil Engineering and Architecture, Zhejiang University, Zhejiang, China.

Elias, S. and Matsagar, V. (2017), "Research developments in vibration control of structures using passive tuned mass dampers", *Ann. Rev. Control*, **44**, 129-156. https://doi.org/10.1016/j.arcontrol.2017.09.015.

Elias, S., Matsagar, V. and Datta, T.K. (2017), "Distributed tuned mass dampers for multi-mode control of benchmark building under seismic excitations", *J. Earthq. Eng.*, **23**(7), 1137-1172. https://doi.org/10.1080/13632469.2017.1351407.

Etedali, S. and Rakhshani, H. (2018), "Optimum design of tuned mass dampers using multi-objective cuckoo search for buildings under seismic excitations", *Alex. Eng. J.*, **57**(4), 3205-3218. https://doi.org/10.1016/j.aej.2018.01.009.

Frans, R. and Arfiadi, Y. (2015), "Designing optimum locations and properties of MTMD systems", *Civ. Eng. Innov. Sustain.*, **125**, 892-898. https://doi.org/10.1016/j.proeng.2015.11.079.

Fujino, Y. (2002), "Vibration, control and monitoring of long-span bridges - recent research, developments and practice in Japan", *J. Constr. Steel Res.*, **58**(1), 71-97. https://doi.org/10.1016/S0143-974X(01)00049-9.

Hansen, P.C. and Oleary, D.P. (1993), "The use of the L-curve in the regularization of discrete ill-posed problems", *Siam J. Sci. Comput.*, **14**(6), 1487-1503. https://doi.org/10.1137/0914086.

Holland, J. (1975), *Adaptation in Natural and Artificial Systems*, University of Michigan Press, Michigan, USA.

Hussan, M., Rahman, M.S., Sharmin, F., Kim, D. and Do, J. (2018), "Multiple tuned mass damper for multi-mode vibration reduction of offshore wind turbine under seismic excitation", *Ocean Eng.*, **160**, 449-460. https://doi.org/10.1016/j.oceaneng.2018.04.041.

Izui, K., Yamada, T., Nishiwaki, S. and Tanaka, K. (2015), "Multiobjective optimization using an aggregative gradient-based method", *Struct. Multidiscipl. Optim.*, **51**(1), 173-182. https://doi.org/10.1007/s00158-014-1125-8.

Jin, Z.L., Yang, Y.W. and Soh, C.K. (2010), "Semi-analytical solutions for optimal distributions of sensors and actuators in smart structure vibration control", *Smart Struct. Syst., Int. J.*, **6**(7), 767-792. https://doi.org/10.12989/sss.2010.6.7.767.

Jin, S.S., Cho, S., Jung, H.J., Lee, J.J. and Yun, C.B. (2014), "A new multi-objective approach to finite element model updating", *J. Sound Vib.*, **333**(11), 2323-2338. https://doi.org/10.1016/j.jsv.2014.01.015.

Kaveh, A., Fahimi-Farzam, M. and Kalateh-Ahani, M. (2015), "Optimum design of steel frame structures considering construction cost and seismic damage", *Smart Struct. Syst., Int. J.*, **16**(1), 1-26. https://doi.org/10.12989/sss.2015.16.1.001.

Lavan, O. (2017), "Multi-objective optimal design of tuned mass dampers", *Struct. Control Health Monit.*, **24**(11), e2008. https://doi.org/10.1002/stc.2008.

Lu, L., Duan, Y.F., Spencer, B.F., Lu, X.L. and Zhou, Y. (2017), "Inertial mass damper for mitigating cable vibration", *Struct. Control Health Monit.*, **24**(10), e1986. https://doi.org/10.1002/stc.1986.

Martí, R. (2003), *Handbook of Metaheuristics*, Springer, Boston, USA.

MathWorks (2020), *Optimization Toolbox User's Guide*, Matlab, USA.

Miguel, L.F.F., Lopez, R.H., Torii, A.J., Miguel, L.F.F. and Beck, A.T. (2016), "Robust design optimization of TMDs in vehicle-bridge coupled vibration problems", *Eng. Struct.*, **126**, 703-711. https://doi.org/10.1016/j.engstruct.2016.08.033.

Nezami, M. and Gholami, B. (2016), "Optimal locations of piezoelectric patches for supersonic flutter control of honeycomb sandwich panels, using the NSGA-II method", *Smart Mater. Struct.*, **25**(3), 035043. https://doi.org/10.1088/0964-1726/25/3/035043.

Niu, H.W., Chen, Z.Q., Hua, X.G. and Zhang, W. (2018), "Mitigation of wind-induced vibrations of bridge hangers using tuned mass dampers with eddy current damping", *Smart Struct. Syst., Int. J.*, **22**(6), 727-741. https://doi.org/10.12989/sss.2018.22.6.727.

Ok, S.Y., Song, J. and Park, K.S. (2008), "Optimal performance design of bi-tuned mass damper systems using multi-objective optimization", *KSCE J. Civ. Eng.*, **12**(5), 313-322. https://doi.org/10.1007/s12205-008-0313-8.

Pourzeynali, S., Salimi, S. and Eimani Kalesar, H. (2013), "Robust multi-objective optimization design of TMD control device to reduce tall building responses against earthquake excitations using genetic algorithms", *Sci. Iran.*, **20**(2), 207-221. https://doi.org/10.1016/j.scient.2012.11.015.

Repetto, M.P. and Solari, G. (2001), "Dynamic alongwind fatigue of slender vertical structures", *Eng. Struct.*, **23**(12), 1622-1633. https://doi.org/10.1016/S0141-0296(01)00021-9.

Siinivas, N. and Deb, K. (1994), "Multiobjective optimization using nondominated sorting in genetic algorithms", *Evol. Comput.*, **2**(3), 221-248. https://doi.org/10.1162/evco.1994.2.3.221.

Tao, T.Y., Wang, H., Yao, C.Y. and He, X.H. (2017), "Parametric sensitivity analysis on the buffeting control of a long-span triple-tower suspension bridge with MTMD", *Appl. Sci. Basel*, **7**(4), 395. https://doi.org/10.3390/app7040395.

Tributsch, A. and Adam, C. (2012), "Evaluation and analytical approximation of tuned mass damper performance in an earthquake environment", *Smart Struct. Syst., Int. J.*, **10**(2), 155-179. https://doi.org/10.12989/sss.2012.10.2.155.

Vellar, L.S., Ontiveros-Perez, S.P., Miguel, L.F.F. and Miguel, L.F.F. (2019), "Robust optimum design of multiple tuned mass dampers for vibration control in buildings subjected to seismic excitation", *Shock Vib.*, **2019**, 9273714. https://doi.org/10.1155/2019/9273714.

Wang, C. and Shi, W.X. (2019), "Optimal design and application of a multiple tuned mass damper system for an in-service footbridge", *Sustainability*, **11**(10), 2801. https://doi.org/10.3390/su11102801.

Wang, D.Y., Wu, C.Q., Zhang, Y.S. and Li, S.W. (2019a), "Study on vertical vibration control of long-span steel footbridge with tuned mass dampers under pedestrian excitation", *J. Constr. Steel Res.*, **154**, 84-98. https://doi.org/10.1016/j.jcsr.2018.11.021.

Wang, Z.H., Gao, H., Xu, Y.W., Chen, Z.Q. and Wang, H. (2019b), "Impact of cable sag on the efficiency of an inertial mass damper in controlling stay cable vibrations", *Smart Struct. Syst., Int. J.*, **24**(1), 83-94. https://doi.org/10.12989/sss.2019.24.1.083.

Wang, L.K., Shi, W.X., Zhou, Y. and Zhang, Q.W. (2020), "Semi-active eddy current pendulum tuned mass damper with variable frequency and damping", *Smart Struct. Syst., Int. J.*, **25**(1), 65-80. http://dx.doi.org/10.12989/sss.2020.25.1.065

Warnitchai, P. and Hoang, N. (2006), "Optimal placement and tuning of multiple tuned mass dampers for suppressing multi-mode structural response", *Smart Struct. Syst., Int. J.*, **2**(1), 1-24. https://doi.org/10.12989/sss.2006.2.1.001.

Xu, K.M. and Igusa, T. (1992), "Dynamic characteristics of multiple substructures with closely spaced frequencies", *Earthq. Eng. Struct. Dyn.*, **21**(12), 1059-1070. https://doi.org/10.1002/eqe.4290211203.

Zahrai, S.M. and Froozanfar, M. (2019), "Performance of passive and active MTMDs in seismic response of Ahvaz cable-stayed bridge", *Smart Struct. Syst., Int. J.*, **23**(5), 449-466. https://doi.org/10.12989/sss.2019.23.5.449.

Zheng, H., Pau, G.S.H. and Wang, Y.Y. (2006), "A comparative study on optimization of constrained layer damping treatment for structural vibration control", *Thin-Wall. Struct.*, **44**(8), 886-896. https://doi.org/10.1016/j.tws.2006.08.005.

Zhou, H.J., Yang, X., Pang, Y.R., Zhou, R., Sun, L.M. and Xing, F. (2019), "Damping and frequency of twin-cables with a cross-link and a viscous damper", *Smart Struct. Syst., Int. J.*, **23**(6), 669-682. https://doi.org/10.12989/sss.2019.23.6.669.

Zi, B., Zhu, Z.C. and Du, J.L. (2011), "Analysis and control of the cable-supporting system including actuator dynamics", *Control Eng. Pract.*, **19**(5), 491-501. https://doi.org/10.1016/j.conengprac.2011.02.001.

HJ